Periodically Twinned Nanowires and Polytypic Nanobelts of ZnS: The Role of Mass Diffusion in Vapor–Liquid–Solid Growth

Yufeng Hao,[§,†] Guowen Meng,*,[§] Zhong Lin Wang,*,[‡] Changhui Ye,[§] and Lide Zhang[§]

Key Laboratory of Materials Physics, and Anhui Key Laboratory of Nanomaterials and Nanostructures, Institute of Solid State Physics, Chinese Academy of Sciences, Hefei, 230031, P R China, Graduate school of Chinese Academy of Sciences, Beijing, 100049, P R China, and School of Materials Science and Engineering, Georgia Institute of Technology, Atlanta, Georgia 30332-0245

ABSTRACT

There are two mass diffusion processes regarding the vapor–liquid–solid (VLS) growth of nanostructures: one is inside the catalyst droplet toward the liquid–solid interface; the other is along the side surface planes of the growing nanostructures. In this letter, microscale, modulated mass diffusion scenarios are exhibited through the synthesis of two types of ZnS nanostructures in an Au-catalyzed VLS process: *periodically twinned nanowires* originated from periodical fluctuation between diffusion rate inside the catalytic droplet and the growth rate on the liquid–solid interface; the formation of *asymmetrically polytypic nanobelts* is related to one certain side surface bounded by high surface-energy plane, which serves as a preferential diffusion direction of reactant adatoms. The results may have important impact on the understanding of the physical and chemical process of the VLS mechanism. These longitudinally and latitudinally tunable crystalline structures enrich the family of one-dimensional nano-building blocks, and may find potential applications in nanotechnology.

One-dimensional (1D) nanostructures, with tunable size, morphology, phase, as well as crystallographic orientation exhibiting distinct physical and chemical performance, are one of the most attractive research fields in today's research in nanotechnology.[1,2] Designing, controlling, and rational growth of 1D nano-architectures with complex structure configurations therefore play a central role in this field.

Vapor–solid (VS) and vapor–liquid–solid (VLS) growth mechanisms are widely applied to steer and interpret the growth of various 1D nanostructures via vapor routes. From the viewpoint of growth kinetics, the VS mechanism emphasizes that surface diffusion of reactant species and preferential incorporation at high-surface-energy sites feed and maintain the continuous growth of nanostructures.[3–6] The process can embody the intrinsic crystallography of materials into nanostructures to form well-faceted structures.[7,8] The VLS mechanism, first found in the early 1960s,[9] has achieved even greater success in recent years for the growth of semiconductor nanowires,[10] nanowire heterostructures,[11]

nanowire superlattices,[12] and hierarchically branched nanowires.[13] In this mechanism, the liquid metallic nanodroplets act as catalysts to adsorb and dissolve reactant species and guide the growth of nanowires with controlled diameters. Four consecutive steps are involved[14] as shown in Figure 1: (1) the adsorption of reactant species on both the catalyst droplet surface and the side surface of growing nanostructures; (2) the dissolution of the species at the droplet surface; (3) the diffusion of the species inside the droplets; and (4) precipitation, incorporation, and crystal growth at the liquid–solid interface. Thus, there are also two types of mass diffusion processes during the VLS growth: one is inside the catalyst droplet and then to the liquid–solid interface; the other is from the side surface of the growing nanostructures toward the catalyst droplet for dissolution.[15] Therefore, the nature of the catalyst droplets and the side surface planes of the growing nanostructures can influence the mass diffusion process. Meanwhile, modulating experimental conditions can also modify the mass diffusion procedure, and thus desired nanostructures can be achieved.

Zinc sulfide (ZnS), an important wide band-gap semiconductor, has two stable phase structures: the cubic zinc blende (CZB) at low temperature and the hexagonal wurtzite (HWZ)

---

* Corresponding authors. E-mail: gwmeng@issp.ac.cn; zhong.wang@mse.gatech.edu.
§ Institute of Solid State Physics, Chinese Academy of Sciences.
† Graduate school of Chinese Academy of Sciences.
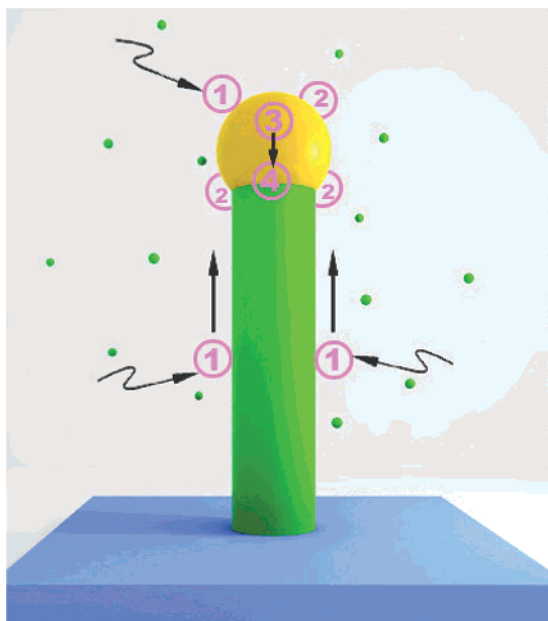‡ Georgia Institute of Technology.

Figure 1. Schematic illustration of detailed, continuous VLS growth steps for 1D nanostructures.

Figure 2. SEM images of two types of ZnS nanostructures. a and b are low- and high-magnification images, respectively. (c) Both types of the nanostructures are terminated by catalytic particles, and the nanobelts show tapering features toward the gold particle. (d) Typical bending contour of a ZnS nanobelt.

at high temperature. A group of 1D ZnS nanostructures, such as nanowires,[16] nanobelts,[17] nanocables,[18] nanotubes,[19] and other morphologies,[20] has been synthesized successfully through high-temperature vapor routes, but most of these structures are dominated by HWZ. In this paper, based on careful exploration of important experimental parameters, we report the synthesis of two types of ZnS nanostructures via an Au-catalyzed VLS process: (1) periodically twinned CZB nanowires (PTNWs) and (2) asymmetrical polytypic nanobelts (APNBs), in which CZB ZnS straight strips parallel to the belt axis were embedded in HWZ nanobelts throughout the entire length. The two types of nanostructures exhibit microscale pictures of mass diffusion inside the catalytic droplet and on the side surface, respectively. Each of them can be simply distinguished by their quite different morphologies although they are obtained under similar conditions of high substrate temperature and high supersaturation ratio.

The synthesis of ZnS nanostructures was performed in a horizontal tube furnace under atmospheric pressure.[6,8,21] ZnS powder (1 g, 99.99%) loaded in an alumina boat was placed in the central heating zone of the alumina tube in the furnace. Several slices of single-crystal Si (100) with a thin gold coating film of ∼5 nm were placed downstream as deposition substrates. Initially, the alumina tube was purged by high purity Ar for 2 h and then the Ar gas was switched off. Second, the system was heated to 1000 °C at 25 °C/min and maintained at this temperature for 5 min. Third, the system was heated to 1200 °C in 1 min and maintained at the peak temperature for another 30 min. During the peak temperature heating, high-purity Ar was introduced into the reaction system as carrier gas at 50 sccm. After the system was cooled naturally, white wool-like or powder-like products grew on the substrates. The morphological and structural features of these products were investigated by field emission scanning electron microscopy (FESEM, SIRION 200, FEI, at 10 kV), transmission electron microscopy (TEM, JEM-2010, JEOL,
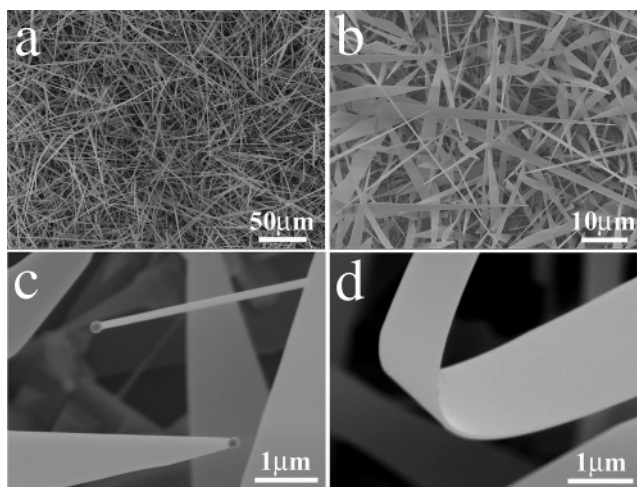
at 200 kV), and energy-dispersive X-ray spectroscopy (EDX, OXFORD, equipped with TEM). In this letter, we focus on the products that are deposited at 1000−1050 °C. There are also other types of ZnS nanostructures at different substrate temperature zones, which are valuable comparisons for understanding the controlled synthesis of desired structures. These structures' characterizations, as well as detailed experimental design and analysis, can be found in the Supporting Information.

Figure 2a and b reveals low- and high-magnification FESEM images of the two kinds of ZnS nanostructures. Detailed observations reveal that a small amount (∼20−30%) of the products is long ZnS nanowires with uniform diameters around 60−100 nm. One of these nanowires can be observed in the upper-right part of Figure 2c. The nanobelts, at a significant percentage (∼70−80%) of the yield, have a typical width of 1−3 μm, a thickness of 40−80 nm (Figure 2d), and lengths of hundreds of micrometers. All of the ZnS nanobelts show tapered morphology toward their ends, where an Au nanoparticle is located at the tip of the nanobelt (lower-left part in Figure 2c). This is distinctly different from previously reported metal oxide or sulfide nanobelts with uniform width that were grown without catalyst.[17]

The products were further characterized by using TEM. Most of the ZnS nanowires (∼90%) reveal sequentially bright/dark contrast stripes throughout the entire length of the wires (Figure 3a, b). Different from hexagonal nanowires reported by several groups, a selected area electron diffraction (SAED, Figure 3c) pattern taken from the wire in Figure 3b shows a CZB structure from the [110] zone axis, indicating the existence of a twin defect along the [111] growth direction. This is the second distinct feature of our samples. A high-resolution TEM image (Figure 3d) further reveals periodically alternating twins along the [111] axis of the wire: atomic sharp twin boundaries appear every 7−9 Zn−S layers. The zigzag angles are 141° (70.5° + 70.5°), in
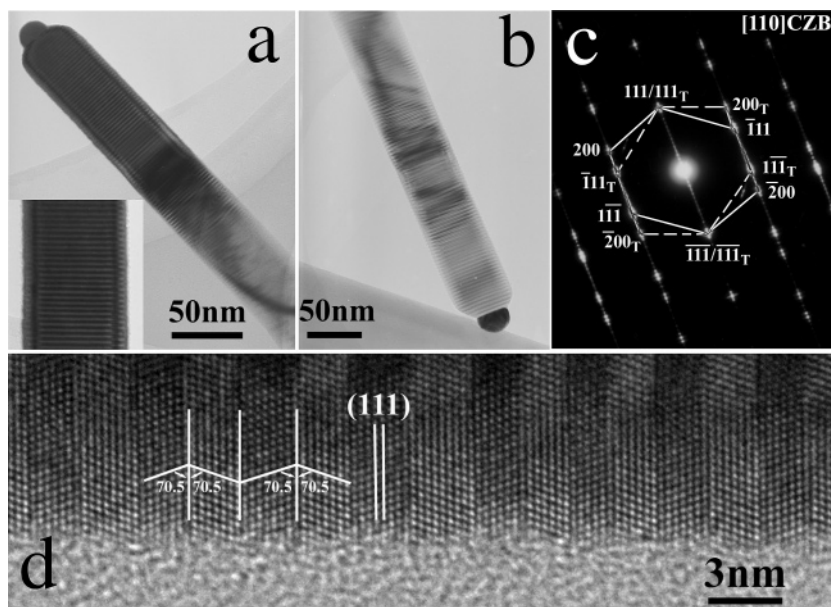
Figure 3. TEM images of PTNWs. a and b are typical alternating bright/dark stripes along the wires. Gold particles are terminated at their ends; the inset in a is a close-up view of the bright/dark stripes in a ZnS wire. (c) SAED pattern recorded from the nanowire in b, showing obvious twinning features labeled by normal and dashed lines. (d) HRTEM image of one nanowire showing periodical twin structures. The amorphous coating on the wire in d is a surface-oxidized sheath.

accordance with the relative rotational angle of (111) twin crystals in face-centered cubic (*fcc*) structures. Twin crystals along {111} facets in *fcc* structures are observed occasionally due to their crystallographic characteristics; however, the occurrence of such ordered twin defects in our PTNWs via VLS growth is considered to be originated from intrinsic successive self-oscillations.[22]

For the ZnS nanobelts, TEM observation reveals a high width-to-thickness ratio and gradually narrowing toward the catalytic nanoparticles at the ends. It is worth noting that straight strips parallel to the belt axis are always embedded inside the belt throughout the entire length, as shown in Figure 4a and b. The typical widths of the strips are 30−50 nm. An SAED pattern (Figure 4c, taken from the belt in Figure 4b) indicates that the nanobelt contains both HWZ and CZB phases. HRTEM images (Figure 4d and e) clearly reveal that the strip (as interlayer) is the CZB phase, whereas the left- and right-hand parts of the strip are HWZ structure. The detailed orientation relationships are HWZ(0001)||CZB-(111) and HWZ[$2\bar{1}\bar{1}0$]||CZB[$0\bar{1}\bar{1}$]. Moreover, the interfaces of the two phases are atomic smooth (Figure 4d). Such a tapered nanobelt looks like an Au-guided nanowire with another segment including HWZ and CZB phases, which grew only on one side of its lateral surface planes of the wire. Our assumption is reasonable because the solubility of an Au droplet is essentially identical during growth; thus, the wires and the tapered segments attached are not initiated only by the gold particle. Taken together, the nanowire grows along the [$01\bar{1}0$] direction and is bounded by orthogonal {$2\bar{1}\bar{1}0$} and ±(0001) planes as side surfaces; a belt-like segment is attached by its {111} facet of CZB strip onto only one basal surface of the HWZ phase, but with the opposite side surface left flat and without growth. As a whole, a well-faceted ZnS APNB is built up, where CZB

and HWZ phases coexist in a single ZnS nanobelt. Generally speaking from the structure point of view, a stacking of ABABAB layers forms a hexagonal structure, whereas a stacking of ABCABC constitutes a cubic phase;[23] in this way, the two phases can be transformed by simply introducing so-called "stacking faults". Although stacking faults sometimes occur in ZnS nanostructures,[17b,20b] and CZB{111} and HWZ{0001} facets are atomically identical, it is rarely seen that planar defects with a high density within a width of nearly 50 nm appear at certain locations, which must be related to some particular growth mode. In addition, EDX spectroscopy analyses indicate that both of the PTNWs and APNBs are composed of Zn and S, whereas Au is present only in the catalytic nanoparticles. No other detectable impurity is found.

It is emphasized that the liquid droplet is a unique characteristic of VLS growth. The above-mentioned detailed steps related to the droplets are the key to the growth procedures and the formation of nanostructures. Under steady-state supply of vapor reactants, either of the last two steps may become rate-determining under different conditions:[24,25] the crystal growth at the liquid−solid interface at low temperature, or the diffusion inside the catalyst droplets at high temperature. In our case, the deposition temperature is high and the crystal growth rate is directly related to the availability of chemical species in the droplet and its diffusion rate through the droplet; thus, a fast growth of the nanowire leads to the depletion of ZnS species in the liquid droplets, which then depresses the crystal growth rates and increases the contact angle between the solution droplet and solid ZnS wire[22] due to reduced wettability at the liquid−solid interface (as shown in Figure 5a and Stage 1 in the schematic model of Figure 5b). Accordingly, under constant supply of vapor reactants, the concentration of chemical species in the droplet
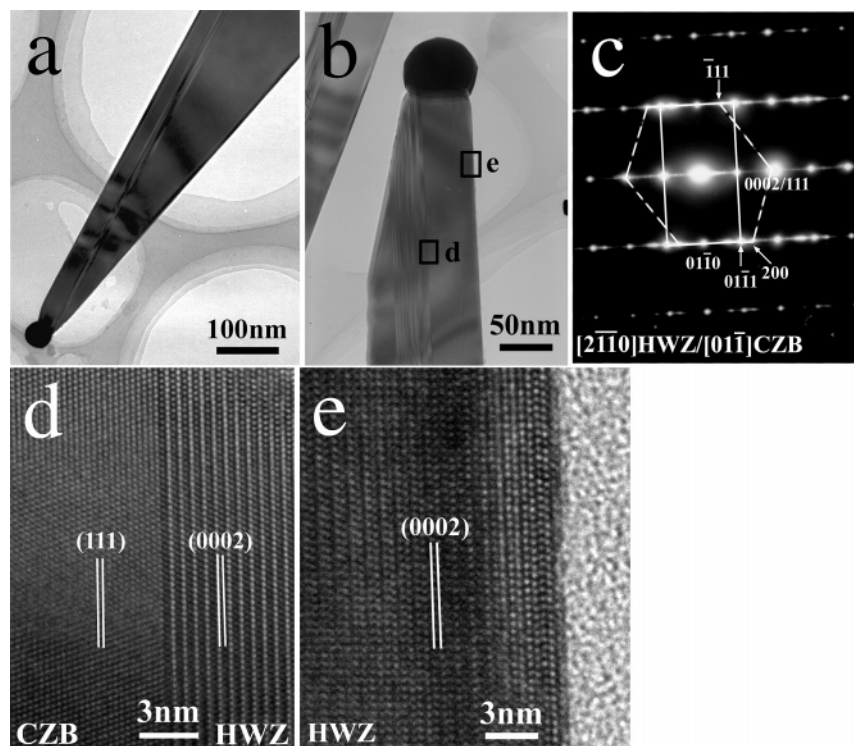
Figure 4. TEM images of ZnS APNBs. a and b are typical polytypic nanobelts at different magnifications. (c) The SAED pattern clearly indicates the coexistence of HWZ and CZB phases, which are denoted by normal and dashed lines, respectively. d and e are HRTEM images from the boxed areas in c, revealing that the gold-assisted HWZ ZnS nanowire is attached by CZB part on only one side surface.

can increase slightly in a little while. As a result, the wettability and growth rate are increased (stage 2). Hence, the next segment of growth is initiated, again leading to depletion in chemical species in the droplet (stage 3). During the entire process, nanowires grow continuously with a periodically modulated growth rate due to the periodic change/modulation of available chemical species in the droplet.[22,26] This process is proposed by assuming that the rate at which the atomic species forms a crystalline structure is faster than the diffusion rate of the chemical species through the catalyst droplet. In the meantime, because of the change in wettability of the liquid−solid interface, the droplet will reshape periodically between nearly spherical and nearly ellipsoidal, followed by successive release of surface and interface energy. Therefore, planar twin defects are formed periodically to release the stored energy.[27,28] Recently, Helveg et al.[29] did observe the periodical reshaping of catalyst particles by in situ imaging the catalyst-induced growth of carbon whiskers. Givargizov[22] and Snoeck et al.[25] also proposed that the shape change could occur during the catalyst-assisted growth of crystal filaments.

Actually, prior to the dissolution at step 2, the reactant adatoms on the side surfaces undergo a "competitive diffusion" process between the liquid droplets and other reactive sites on the side surface. Generally, owing to the ideal roughness[22] of liquid droplets, most adatoms will be dissolved into the droplet through side-surface diffusion.[15] Nanostructures grown via the VLS mechanism are therefore characterized by wire-like morphologies because their side surfaces are bounded by low-energy facets. However, HWZ ZnS can be described schematically as alternating stacking

of positive (0001)-Zn and negative (000$\bar{1}$)-S layers along the polarized C axis,[20a] much similar to the widely studied hexagonal ZnO, [30] in which the (0001)-Zn plane is chemically more active than the (000$\bar{1}$)-O plane and the surface energy of the (0001)-Zn plane is the highest among those of all of the low-index crystal planes. Thus, for HWZ ZnS nanowires growing along the [01$\bar{1}$0] direction (Figure 5c), both the droplets and the chemically active (0001)-Zn side surface planes simultaneously become two preferential diffusion directions to exhibit the competitive process and initiate the tapered nanobelt growth under a relatively high supersaturation ratio. Compared with the growth of the high-temperature stable HWZ wires through the intermediate dissolution and precipitation in droplets (this process normally reduces barriers for chemical reaction and reduces the activation energy of nucleation[14]), direct sink and fast incorporation of adatoms on the (0001)-Zn side surface planes usually favor the high-temperature metastable CZB phase, which is kinetically controlled.[31] The segments growing without the assistance of droplets, nevertheless, tend to form a thermodynamics-favored HWZ phase at such high deposition temperatures, which is analogous to the case for ordinary ZnS nanobelts through the VS process (Supporting Information Figure S4). Thereby, the CZB dominates merely at confined locations of APNBs. However, the occurrence of the CZB phase is also evidence corroborating our viewpoint of surface diffusion.[32] At this stage, one question still remains open: What is the driving force to the original phase selection for the two types of nanostructures? This issue may be related to the different sizes of catalytic droplets and should be elucidated in the future.
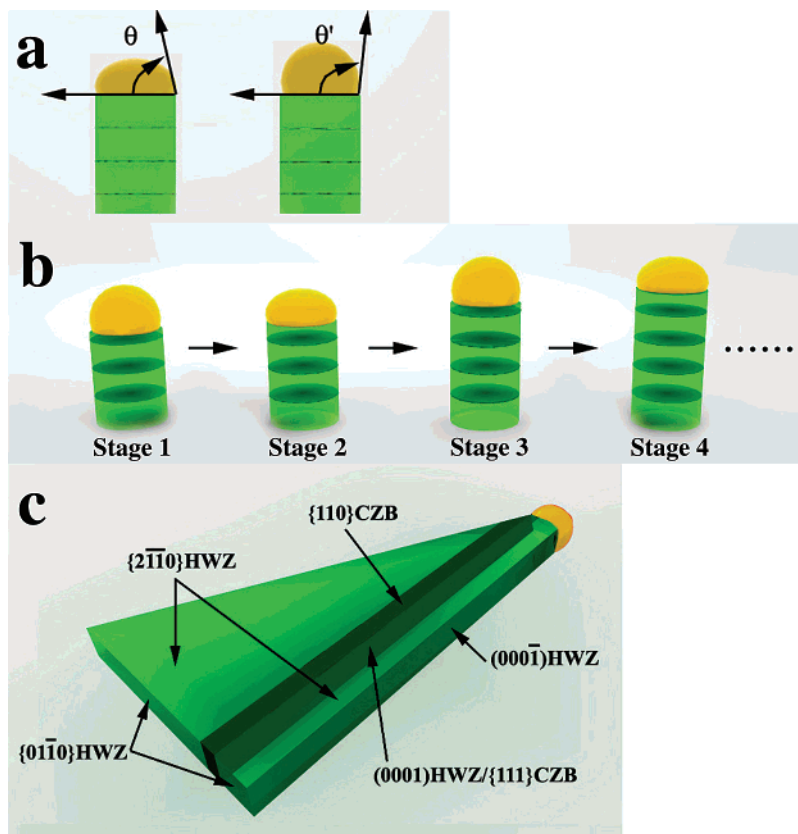
Figure 5. (a) The variation of contact angle (θ) with regard to liquid-solid interface wettability. b and c are schematic models for the formation of ZnS PTNWs and APNBs, respectively. Twin boundaries are indicated by dark green slices in b.

In summary, through adjusting synthesis parameters, ZnS PTNWs and APNBs have been synthesized via Au-assisted VLS processes. The formation of the two types of ZnS nanostructures is based on modulating mass diffusion procedures in the catalyst droplet and on the nanowire side surfaces, respectively. Considering the popularity of CZB and HWZ phases in a number of II−VI and III−V group functional materials,[23] rational growth of similar nanostructures of other materials is also prospective. These longitudinally and transversal tunable crystalline structures enrich the family of 1D nano-building blocks, may induce distinctive electron and phonon scattering, and find potential applications in electronics, optoelectronics, and thermoelectronics.

Supporting Information Available: Detailed experimental design and parameter adjusting are provided. SEM and TEM images of these products are presented. This material is available free of charge via the Internet at http://pubs.acs.org.

References

(1) Xia, Y.; Yang, P.; Sun, Y.; Wu, Y.; Mayers, B.; Gates, B.; Yin, Y.; Kim, F.; Yan, H. *Adv. Mater.* **2003**, *15*, 353.

(2) Burda, C.; Chen, X.; Narayanan, R.; El-Sayed, M. A. *Chem. Rev.* **2005**, *105*, 1025.

(3) (a) Sears, G. W. *Acta Metall.* **1955**, *4*, 361. (b) Sears, G. W. *Acta Metall.* **1955**, *4*, 367.

(4) Ruth, V.; Hirth, J. P. *J. Chem. Phys.* **1964**, *41*, 3139.

(5) Dai, Z. R.; Pan, Z. W.; Wang, Z. L. *Adv. Funct. Mater.* **2003**, *13*, 9.

(6) Ye, C. H.; Fang, X.; Hao, Y. F.; Teng, X. M.; Zhang, L. D. *J. Phys. Chem. B* **2005**, *109*, 19758.

(7) (a) Pan, Z. W.; Dai, Z. R.; Wang, Z. L. *Science* **2001**, *291*, 1947. (b) Gao, P. X.; Ding, Y.; Mai, W.; Hughes, W. L.; Lao, C.; Wang, Z. L. *Science* **2005**, *309*, 1700.

(8) (a) Hao, Y. F.; Meng, G. W.; Ye, C. H.; Zhang, X. R.; Zhang, L. D. *J. Phys. Chem. B* **2005**, *109*, 11204. (b) Hao, Y. F.; Meng, G. W.; Ye, C. H.; Zhang, L. D. *Cryst. Growth Des.* **2005**, *5*, 1617.

(9) Wagner, R. S.; Ellis, W. C. *Appl. Phys. Lett.* **1964**, *4*, 89.

(10) Morales, A. M.; Lieber, C. M. *Science* **1998**, *279*, 208.

(11) Hu, J.; Ouyang, M.; Yang, P.; Lieber, C. M. *Nature* **1999**, *399*, 48.

(12) (a) Gudiksen, M. S.; Lauhon, L. J.; Wang, J.; Smith, D. C.; Lieber, C. M. *Nature* **2002**, *415*, 617. (b) Wu, Y.; Fan, R.; Yang, P. *Nano Lett.* **2002**, *2*, 83. (c) Bjork, M. T.; Ohlssen, B. J.; Sass, T. P.; Thelander, A. I. C.; Magnusson, M. H.; Deppert, K.; Wallenberg, L. R.; Samuelson, L. *Nano Lett.* **2002**, *2*, 87.

(13) (a) Dick, K.; Deppert, K.; Larsson, M. W.; Martensson, T.; Seifert, W.; Wallenberg, L.; Samuelson, L. *Nat. Mater.* **2004**, *3*, 380. (b) Wang, D.; Qian, F.; Yang, C.; Zhong, Z.; Lieber, C. M. *Nano Lett.* **2004**, *4*, 871.

(14) Givargizov, E. I. *J. Cryst. Growth* **1975**, *31*, 20.

(15) Jensen, L. E.; Bjork, M. T.; Jeppesen, S.; Persson, A. I.; Ohlsson, B. J.; Samuelson, L. *Nano Lett.* **2004**, *4*, 1961.

(16) (a) Wang, Y. W.; Zhang, L. D.; Liang, C. H.; Wang, G. Z.; Peng, X. S. *Chem. Phys. Lett.* **2002**, *357*, 314. (b) Xiong, Q.; Chen, G.; Acord, J. D.; Liu, X.; Zengel, J. J.; Gutierrez, H. R.; Redwing, J. M.; Lew

Yan Voon, L. C.; Lassen, B.; Eklund, P. C. *Nano Lett.* **2004**, *4*, 1663. (c) Kar, S.; Chaudhuri, S. *J. Phys. Chem. B* **2005**, *109*, 3298. (d) Cheng, B.; Wang, Z. *Adv. Funct. Mater.* **2005**, *15*, 1883.

(17) (a) Ye, C. H.; Fang, X.; Li, G. H.; Zhang, L. D. *Appl. Phys. Lett.* **2004**, *85*, 3035. (b) Ding, Y.; Wang, X. D.; Wang, Z. L. *Chem. Phys. Lett.* **2004**, *398*, 32. (c) Jiang, Y.; Meng, X. M.; Liu, J.; Xie, Z. Y.; Lee, C. S.; Lee, S. T. *Adv. Mater.* **2003**, *15*, 323. (d) Jiang, Y.; Meng, X. M.; Liu, J.; Hong, Z.; Lee, C. S.; Lee, S. T. *Adv. Mater.* **2003**, *15*, 1195. (e) Liang, C.; Shimizu, Y.; Sasaki, T.; Umehara, H.; Koshizaki, N. *J. Phys. Chem. B* **2004**, *108*, 9728. (f) Zhang, Z.; Wang, J.; Yuan, H.; Gao, Y.; Liu, D.; Song, L.; Xiang, Y.; Zhao, X.; Liu, L.; Luo, S.; Dou, X.; Mou, S.; Zhou, W.; Xie, S. *J. Phys. Chem. B* **2005**, *109*, 18352.

(18) Wang, X.; Gao, P.; Li, J.; Summers, C. J.; Wang, Z. L. *Adv. Mater.* **2002**, *14*, 1732.

(19) (a) Hu, J.; Bando, Y.; Zhan, J.; Golberg, D. *Angew. Chem., Int. Ed.* **2004**, *43*, 4606. (b) Yin, L.; Bando, Y.; Zhan, J.; Li, M.; Golberg, D. *Adv. Mater.* **2005**, *17*, 1972.

(20) (a) Moore, D.; Ronning, C.; Ma, C.; Wang, Z. L. *Chem. Phys. Lett.* **2004**, *385*, 8. (b) Ma, C.; Moore, D.; Li, J.; Wang, Z. L. *Adv. Mater.* **2003**, *15*, 228.

(21) Hao, Y. F.; Meng, G. W.; Ye, C. H.; Zhang, L. D. *Appl. Phys. Lett.* **2005**, *87*, 033106.

(22) Givargizov, E. I. *J. Cryst. Growth* **1973**, *20*, 217.

(23) Yeh, C. Y.; Lu, Z. W.; Froyen, S.; Zunger, A. *Phys. Rev. B* **1992**, *46*, 10086.

(24) Bakkers, E. P. A. M.; Verheijen, M. A. *J. Am. Chem. Soc.* **2003**, *125*, 3440.

(25) Snoeck, J. W.; Froment, G. F.; Fowlesz, M. *J. Catal.* **1997**, *169*, 240.

(26) Compared with the observation by Givargizov,[21] there is no obvious diameter change for PTNWs in our observation, which may be caused by slight shape change of the liquid droplets, and the formation of surface-sheathed oxidized layers (Figure 3a, b, and d), that further weaken the diameter variations.

(27) Li, Q.; Gong, X.; Wang, C.; Wang, J.; Ip, K.; Hark, S. *Adv. Mater.* **2004**, *16*, 1436.

(28) {111} facets of the CZB structure are a prerequisite to the formation of twins, which eliminates the possibility of twins appearing in nanowires with other orientations or the HWZ phase.

(29) (a) Helveg, S.; Lo'pez-Cartes, C.; Sehested, J.; Hansen, P. L.; Clausen, B. S.; Rostrup-Nielsen, J. R.; Abild-Pedersen, F.; Nørskov, J. K. *Nature* **2004**, *427*, 426. (b) Ajayan, P. M. *Nature* **2004**, *427*, 402.

(30) (a) Wang, Z. L.; Kong, X. Y.; Zuo, J. M. *Phys. Rev. Lett.* **2003**, *91*, 185502. (b) Wang, Z. L. *J. Phys.: Condens. Matter* **2004**, *16*, R829.

(31) Ito, T. *Jpn. J. Appl. Phys. 2* **1998**, *37*, L1217−L1220.

(32) Side surfaces of PTNWs are generally bounded by low-energy facets, such as {110}. Therefore, the effect of surface diffusion for PTNWs is very weak under the current experimental conditions.